Letter to the Editor

Imaging biomarkers between primary and metastatic tumors revealed by total-body positron emission tomography/computed tomography-based radiomics: a case series

Jianghao Li[1], Jianfeng Qiu[1], Zhaoping Cheng[2], Weizhao Lu[1]^

[1]School of Radiology, Shandong First Medical University & Shandong Academy of Medical Sciences, Tai'an, China; [2]Department of PET-CT, the First Affiliated Hospital of Shandong First Medical University, Shandong Provincial Qianfoshan Hospital Affiliated to Shandong University, Jinan, China

Correspondence to: Zhaoping Cheng, MD. Department of PET-CT, the First Affiliated Hospital of Shandong First Medical University, Shandong Provincial Qianfoshan Hospital Affiliated to Shandong University, No. 16766 Jingshi Road, Jinan 250014, China. Email: czpabc@163.com; Weizhao Lu, MD. School of Radiology, Shandong First Medical University & Shandong Academy of Medical Sciences, No. 619 Changcheng Road, Tai'an 271000, China. Email: mingming9053@163.com.

Submitted Jan 04, 2024. Accepted for publication Apr 23, 2024. Published online May 24, 2024.
doi: 10.21037/qims-24-21
View this article at: https://dx.doi.org/10.21037/qims-24-21

Introduction

Despite significant developments in the field of tumor treatment, tumor metastasis remains an important cause of death in patients (1). Currently, most tumor treatments are based on the primary tumor (2). However, in the situation where tumors are found in one or more metastatic sites, yet the primary site cannot be determined, it is difficult to implement effective treatments (3). Therefore, determining the primary location of the metastatic tumor is of clinical significance (4-7).

Currently, total-body positron emission tomography/computed tomography (PET/CT) has provided a new path for localizing the primary site of metastatic tumors (8,9). One study applied whole-body multiparametric imaging to extract regional time-activity curves (TAC) of suspicious lesions from 5 patients with metastatic genitourinary cancer, and found that within the same patient, multiple metastatic lesions exhibited similar TAC shapes (8). Another case study used static total-body positron emission tomography (PET) examination to pinpoint possible locations with abnormal glucose uptake, and used dynamic total-body PET scan to reveal the metabolic association between the metastatic tumor and possible primary tumors (10). However, the majority of previous studies have used dynamic or parametric total-body PET imaging to establish the association between primary and metastatic tumors (8,10). One significant limitation of dynamic PET examination is its prolonged acquisition duration, which often hinders patient cooperation and is susceptible to physiological movements. Therefore, this case series study aims to search for imaging markers between primary and metastatic tumors based on static whole-body PET/CT imaging and radiomics.

Case presentation

In this case series, we collected two patients with pathologically verified metastases. The detailed information for the two patients are as follows. All procedures performed in this study were in accordance with the Ethics Committee of Shandong First Medical University and with the Helsinki Declaration (as revised in 2013). Written informed consent was obtained from the patient for publication of this article and accompanying images. A copy of the written consent is available for review by the editorial office of this journal.

Patient 1

A 50-year-old woman presented to the hospital with

^ ORCID: 0000-0002-2941-9791.

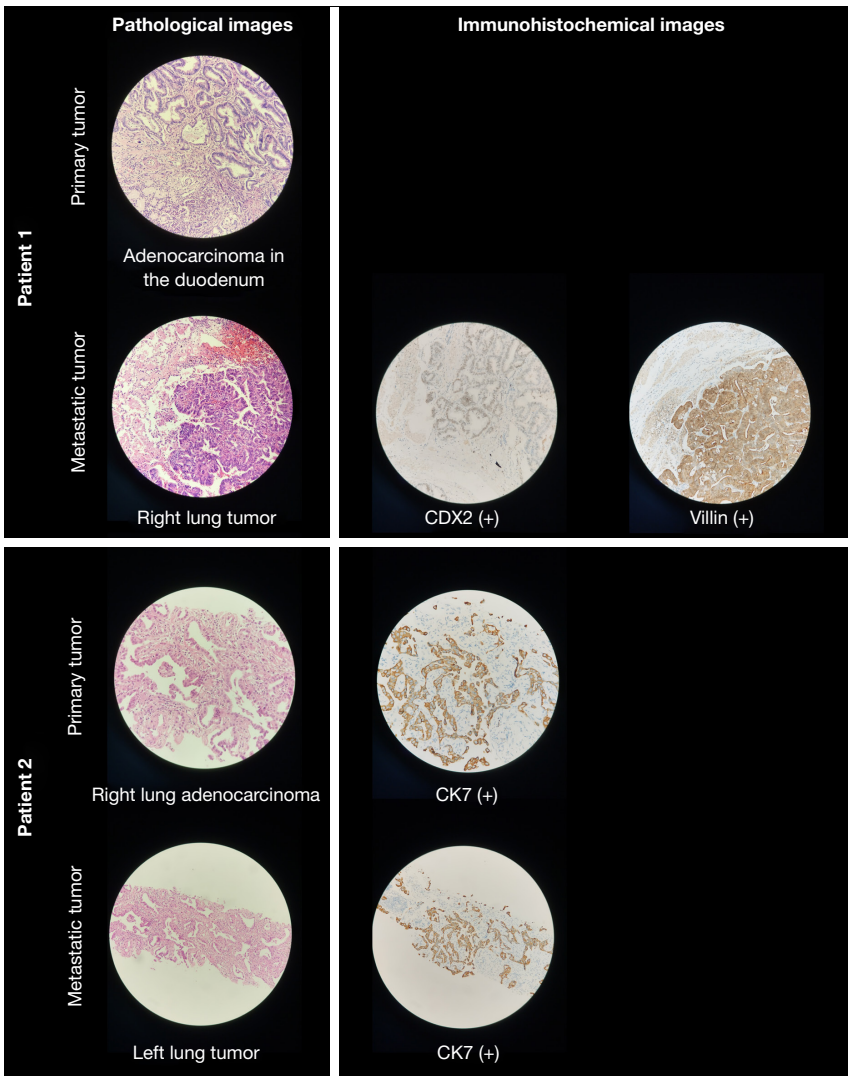

Figure 1 Pathological and immunohistochemical examination of the specimen from the primary and metastatic tumors for the two patients. Pathological images are H&E stained. All images are ×400 original magnification. CDX2, caudal type homeobox 2; CK7, cytokeratin-7; H&E, hematoxylin and eosin.

symptoms including yellowing of the skin, mucous membranes, and sclera for no apparent reasons. Through imaging examinations, we found that the patient's wall of the duodenum was thickened, with the thickest area of about 2.7 cm. In addition, a soft tissue mass of about 1.7×1.2×1.9 cm^3 was seen in the apical zone of the right lung, showing "ground glass-like" changes around the lesion. The edge of the lesion was surrounded by spicules with adjacent pleural adhesions. Computed tomography (CT) value of the right lung lesion was about 29 HU. Postoperative pathology showed that the patient had a duodenal papillary adenocarcinoma, and an intestinal adenocarcinoma component in the apical zone of the right lung. Immunohistochemical test of the right lung lesion revealed positive results for caudal type homeobox 2 (CDX2) and Villin, and weak positive results for β-Tubulin-3 and Topoisomerase II alpha (TOPO2A), and negative results for cytokeratin-20 (CK20), cytokeratin-7 (CK7), thyroid transcription factor-1 (TTF-1), Napsin A and tumor protein 63 (p63) (*Figure 1*). Combined with medical history and immunohistochemistry results, the lesion located in the right lung was diagnosed as the metastatic tumor from the

duodenal adenocarcinoma.

Patient 2

A 44-year-old man who had a lung occupancy for more than five months presented to the hospital with chest tightness for no apparent causes. CT scan of the chest showed a glass nodule with a maximum cross-section of 2.5×1.9 cm^2 in the lower lobe of the right lung, with lobulated shape, spiculation sign, and adhesion of the pleura. Chest CT also demonstrated multiple nodules in the bilateral lungs, some of which showed ground glass-like changes. The largest nodule was located in the lower lobe of the left lung, approximately 0.9 cm in diameter, with no significant change compared to previous examinations. Postoperative pathology confirmed that the right lung tumor exhibited features consistent with adnexal-like predominant adenocarcinoma, characterized by immunohistochemical positivity for CK7 and negativity for p63. Furthermore, pathological examination revealed that the largest nodule in the left lung was also adenocarcinoma, primarily exhibiting an adnexal-like growth pattern, with similar immunohistochemical findings of CK7 positivity and p63 negativity (as illustrated in *Figure 1*). Therefore, the right lung tumor was diagnosed as the primary focus and the left lung tumor as the metastatic focus.

Total-body PET/CT imaging and radiomics analysis

Total-body PET/CT imaging examination

The two patients underwent total-body PET/CT imaging examination. After fast for at least 6 hours, ^{18}F-flurodeoxyglucose (^{18}F-FDG) was injected through a vein near the patients' ankle according to the patients' weight (2.96 MBq/kg). Fifty minutes after the injection, static total-body PET scan with a duration of 600 s was performed using the uEXPLORER (United Imaging, China). PET images were reconstructed using all 600-s data, time of flight and point spread function modeling, 2 iterations and 20 subsets, matrix =192×192, slice thickness =2.89 mm, voxel size =3.125×3.125×2.886 mm^3 with a Gaussian filter (FWHM =3 mm), and all necessary corrections were performed, including attenuation and scattering correction. In addition, whole-body high-resolution CT scans were performed. The parameters were: voltage =120 kVp, matrix =512×512, slice thickness =1.5 cm, with reconstructed voxel size of 0.9766×0.9766×1.5000 mm^3.

For Patient 1, total-body PET imaging revealed thickened duodenal wall, with significantly increased ^{18}F-FDG uptake (SUV_{max} =33.2). An occupying lesion in the upper lobe of the right lung with markedly elevated metabolism (SUV_{max} =43.0) was found (*Figure 2A*). In terms of Patient 2, PET/CT exam showed a mixed glass foci in the dorsal segment of the right lower lung with increased ^{18}F-FDG uptake (SUV_{max} =4.6), a solid nodular foci in the dorsal segment of the left lower lung with increased ^{18}F-FDG uptake (SUV_{max} =5.6) (*Figure 2B*). However, at present stage, no further information from the foci can be obtained from the static total-body PET/CT images.

Total-body PET/CT-based radiomics

The total-body PET/CT images were then used for radiomics analysis. 3D region of interests (ROIs) of the primary and metastatic tumors were delineated via ITK-SNAP (version 3.8.0). Pyradiomics (version 3.0.1) based on Python (version 3.6.0) was used to extract 18 voxel-wise first-order feature (histogram-based) maps from both PET and CT images (11). The features included 10 percentile, 90 percentile, energy, entropy, interquartile range, kurtosis, maximum, mean, mean absolute deviation, median, minimum, range, robust mean absolute deviation, root mean squared, skewness, total energy, uniformity, variance.

We assessed the similarity of voxel-wise feature maps for primary and metastatic tumors from the same imaging modality (PET or CT images) of the same patient using the histogram comparison function in the OpenCV (version 4.7.0) (12). Specifically, histograms of voxel-wise feature maps were obtained via 256 bins from the minimum to the maximum value. The bin number was determined taken the range of the feature maps and consistency across PET and CT images into consideration. However, sparsity might occur in some bins of the histogram. Histogram similarity between the primary and metastatic tumors from the same imaging modality (PET or CT images) of the same patient was evaluated using four metrics, namely, correlation, chi-square, intersection and Bhattacharyya distance.

We found that kurtosis maps had higher correlation coefficient and intersect, and lower chi-square value and Bhattacharyya distance between primary and metastatic tumors compared with other radiomics feature maps both in CT images and in PET images (*Figure 3*), which might stand a chance to be the potential imaging marker to discover the association between metastatic and primary tumors, and thus to localize the location of the primary tumor. *Figure 4* visualizes kurtosis feature maps and relevant histograms for the PET and CT images from the two

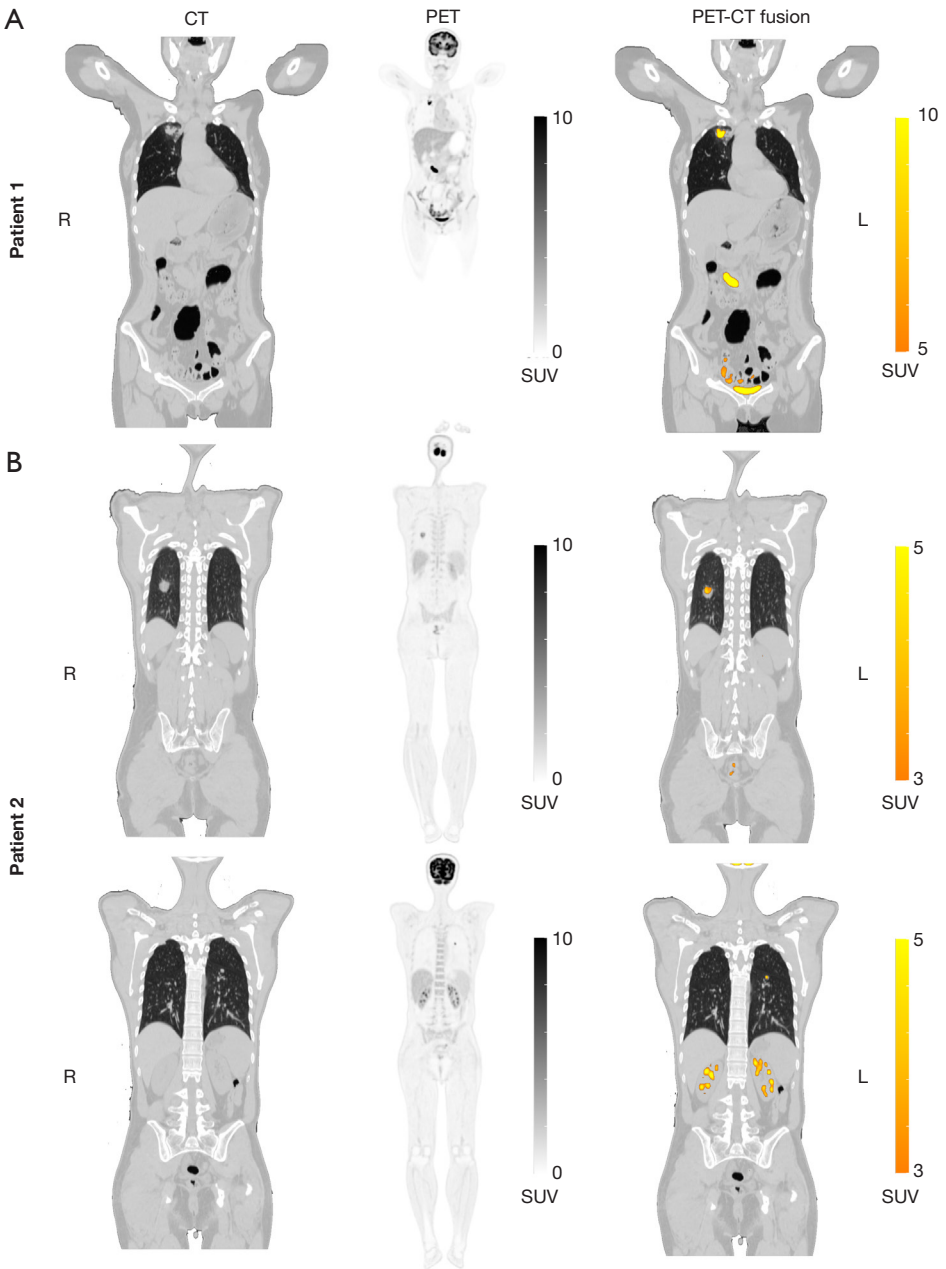

Figure 2 Total-body PET/CT images for the two patients. CT, PET and PET/CT fused images for (A) Patient 1 and (B) Patient 2. The color bar indicates SUV. CT, computed tomography; PET, positron emission tomography; SUV, standardized uptake value.

patients (Figures S1-S4 display the histograms of the rest radiomics feature maps).

Discussion

In this case series study, we collected two cases with pathology-confirmed primary and metastatic tumors. We performed a total-body PET/CT examination, and extracted various radiomics features of metastatic and primary tumors from PET and CT images, respectively. We found possible connections in the kurtosis feature maps between primary and metastatic tumors by similarity analysis of histograms, which laid the foundation for the localization of the primary foci using total-body PET/CT

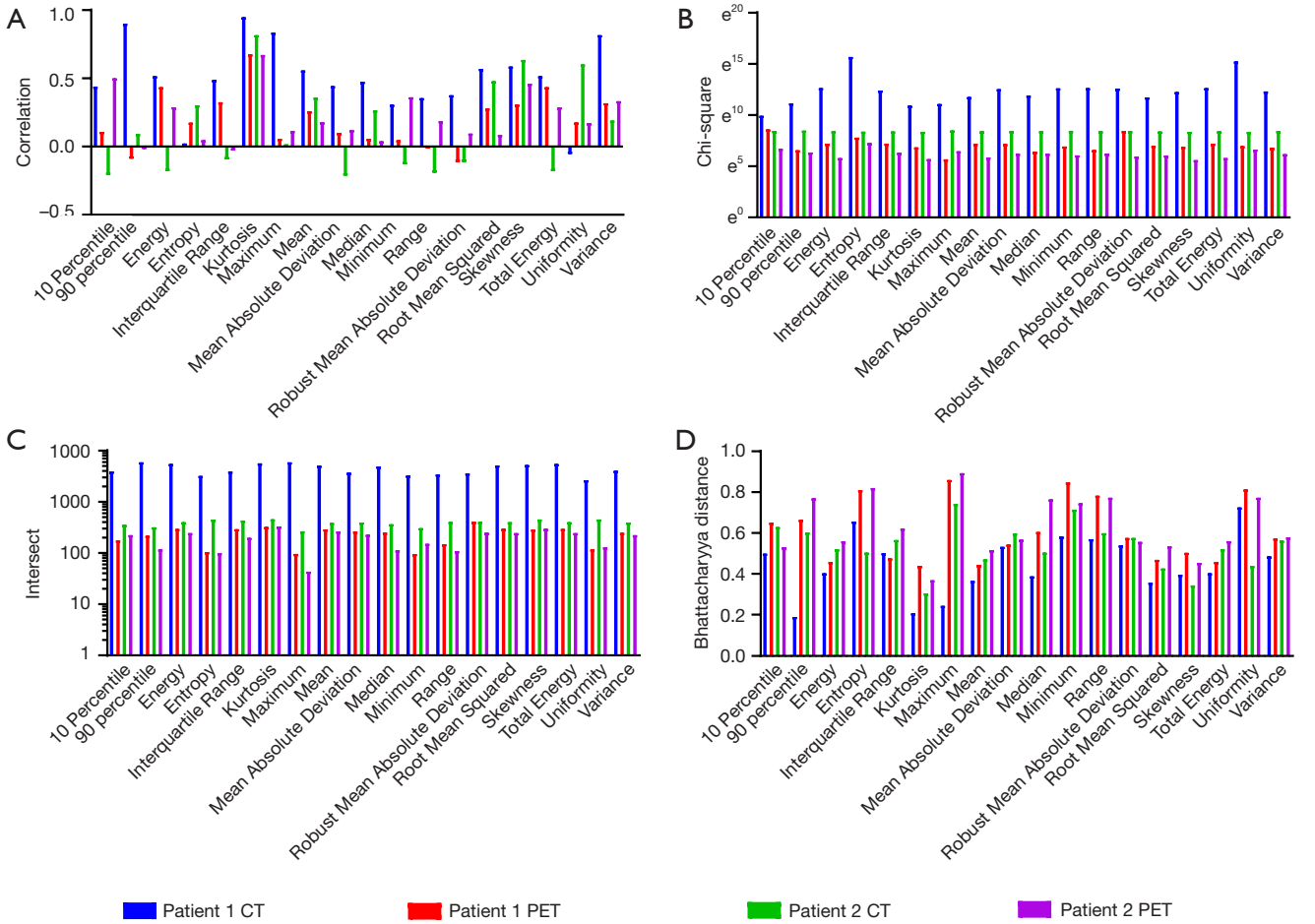

Figure 3 Similarity results between primary and metastatic tumors from the same imaging modality from the same patients. (A) Correlation coefficient. (B) Chi-square. (C) Intersect. (D) Bhattacharyya distance. CT, computed tomography; PET, positron emission tomography.

imaging in the future.

While dynamic total-body PET/CT technique has shown a potential value in the localization of primary tumor (8,10), its practical application is hindered by the prohibitively long acquisition time. Therefore, we aimed to use the less time-consuming static total-body PET/CT scan to determine the primary tumor. Furthermore, previous studies have demonstrated that the primary tumor and the metastasis have similar metabolic and textural features (10,13,14). Therefore, we tried to find possible associations from total-body PET/CT images via voxel-wise radiomics analysis, which could further lead to the determination of the primary tumor. Taken computational burden and interpretability into consideration, only first-order feature maps were extracted in the current case series.

Our study revealed high similarities in kurtosis feature maps between the primary and metastatic lesions in both CT and PET images. Kurtosis is a textural feature used to describe the characteristics of gray value distribution (15). In terms of cancer imaging, kurtosis has been shown to be strongly associated with clinical outcomes (16). In addition, a previous study has also demonstrated that kurtosis features from PET and CT images can be used to characterize histotypes of lung cancer (17). In line with previous findings (10,13,14), the similarity of kurtosis feature maps can be interpreted as the similarity in metabolic profiles and textural characteristics between metastatic and primary cancers, which in turn have the potential to be used as imaging biomarkers for the localization of primary tumors.

Compared to previous studies using total-body dynamic PET/CT scan to explore the association between primary and metastatic tumors, dynamic PET scan takes longer time

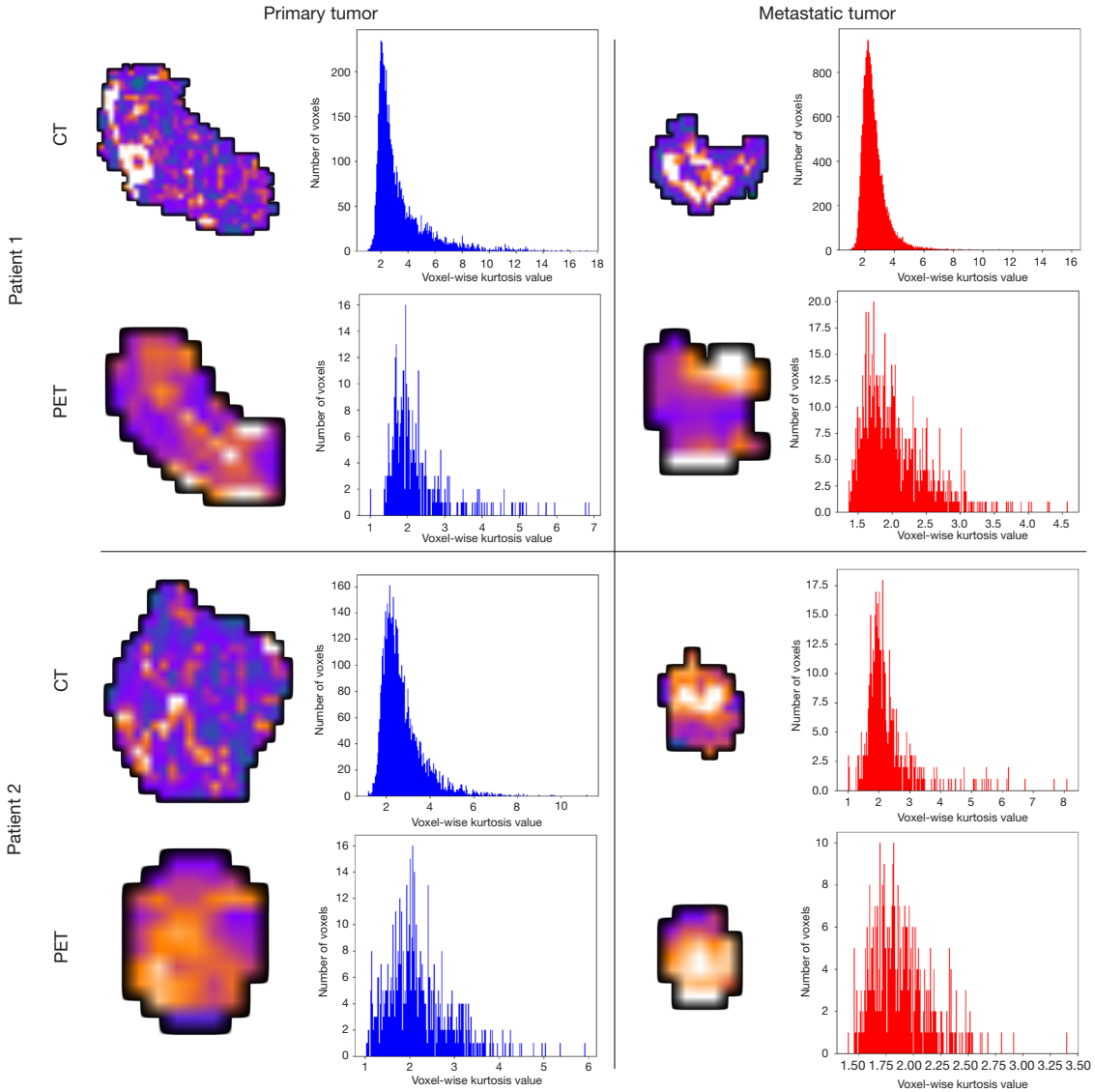

Figure 4 Kurtosis feature maps and the corresponding histograms from tumor CT and PET images for the two patients. CT, computed tomography; PET, positron emission tomography.

(always more than one hour) and has a lower signal-to-noise ratio (8,10). In contrast, the case series in this study used static PET/CT scan, which is less time-consuming (usually 10 minutes). Via certain radiomics feature such as kurtosis, static PET/CT scan is expected to find the primary tumor rapidly and precisely. In addition, this study calculated voxel-wise image features rather than ROI-wise image features, which is expected to play a greater role in finding the primary focus across the human body.

In conclusion, we collected two cases with pathology-confirmed primary and metastatic tumors. We performed total-body PET/CT examination, and extracted various radiomics features for metastatic and primary tumors from PET and CT images, respectively. We found possible connections in the kurtosis feature maps between primary and metastatic tumors by similarity analysis of histograms. The method proposed by this study demonstrates promise in locating the primary focus of metastatic tumors to achieve a better clinical diagnosis. However, a major limitation of this study is the lack of clinical samples. Future studies with larger samples are needed to validate the generalizability of the current case series.

Acknowledgments

Funding: This study received funding by the Taishan Scholars Program of Shandong Province (Grant No. TS201712065 to J.Q.), Academic Promotion Program of Shandong First Medical University (Grant No. 2019QL009 to J.Q.), Science and Technology funding from Jinan (Grant No. 2020GXRC018 to J.Q.), and Natural Science Foundation of Shandong Province (Grant No. ZR2023QH109 to W.L.).

Footnote

Conflicts of Interest: All authors have completed the ICMJE uniform disclosure form (available at https://qims.amegroups.com/article/view/10.21037/qims-24-21/coif). J.Q. reports funding from the Taishan Scholars Program of Shandong Province (Grant No. TS201712065), Academic Promotion Program of Shandong First Medical University (Grant No. 2019QL009), Science and Technology funding from Jinan (Grant No. 2020GXRC018). W.L. reports funding from the Natural Science Foundation of Shandong Province (Grant No. ZR2023QH109). The other authors have no conflicts of interest to declare.

Ethical Statement: The authors are accountable for all aspects of the work in ensuring that questions related to the accuracy or integrity of any part of the work are appropriately investigated and resolved. All procedures performed in this study were in accordance with the Ethics Committee of Shandong First Medical University and with the Helsinki Declaration (as revised in 2013). Written informed consent was obtained from the patient for publication of this article and accompanying images. A copy of the written consent is available for review by the editorial office of this journal.

References

1. Mehlen P, Puisieux A. Metastasis: a question of life or death. Nat Rev Cancer 2006;6:449-58.
2. Lu MY, Chen TY, Williamson DFK, Zhao M, Shady M, Lipkova J, Mahmood F. AI-based pathology predicts origins for cancers of unknown primary. Nature 2021;594:106-10.
3. Varadhachary GR, Raber MN. Cancer of unknown primary site. N Engl J Med 2014;371:757-65.
4. Curcean A, Curcean S, Rescigno P, Dafydd DA, Tree A, Reid A, Koh DM, Sohaib A, Tunariu N, Shur J. Imaging features of the evolving patterns of metastatic prostate cancer. Clin Radiol 2022;77:88-95.
5. Lind P, Igerc I, Beyer T, Reinprecht P, Hausegger K. Advantages and limitations of FDG PET in the follow-up of breast cancer. Eur J Nucl Med Mol Imaging 2004;31 Suppl 1:S125-34.
6. Tan H, Gu Y, Yu H, Hu P, Zhang Y, Mao W, Shi H. Total-Body PET/CT: Current Applications and Future Perspectives. AJR Am J Roentgenol 2020;215:325-37.
7. Zhang YQ, Hu PC, Wu RZ, Gu YS, Chen SG, Yu HJ, Wang XQ, Song J, Shi HC. The image quality, lesion detectability, and acquisition time of 18F-FDG total-body PET/CT in oncological patients. Eur J Nucl Med Mol Imaging 2020;47:2507-15.
8. Wang G, Nardo L, Parikh M, Abdelhafez YG, Li E, Spencer BA, Qi J, Jones T, Cherry SR, Badawi RD. Total-Body PET Multiparametric Imaging of Cancer Using a Voxelwise Strategy of Compartmental Modeling. J Nucl Med 2022;63:1274-81.
9. Nardo L, Abdelhafez YG, Spencer BA, Badawi RD. Clinical Implementation of Total-Body PET/CT at University of California, Davis. PET Clin 2021;16:1-7.
10. Lu W, Qiu J, Xie X, Li K, Duan Y, Li M, Ma C, Cheng Z, Liu S. Recognizing Tumor Origin for Lymphoid Tumor of Unknown Primary via Total-Body PET/CT Scan-Case Report. Front Oncol 2022;12:766490.
11. van Griethuysen JJM, Fedorov A, Parmar C, Hosny A, Aucoin N, Narayan V, Beets-Tan RGH, Fillion-Robin JC, Pieper S, Aerts HJWL. Computational Radiomics System to Decode the Radiographic Phenotype. Cancer Res 2017;77:e104-7.
12. Bradski G. The OpenCV Library. Dr. Dobb's Journal of Software Tools 2000;120:122-5.
13. Gupta P, Rana P, Ganeshan B, Kalage D, Irrinki S, Gupta

V, Yadav TD, Kumar R, Das CK, Gupta P, Endozo R, Nada R, Srinivasan R, Kalra N, Dutta U, Sandhu M. Computed tomography texture-based radiomics analysis in gallbladder cancer: initial experience. Clin Exp Hepatol 2021;7:406-14.
14. Nishimura M, Tamaki N, Matsushima S, Kiba M, Kotani T, Bamba C, Nakamura Y, Yamada K. Dynamic whole-body (18)F-FDG PET for differentiating abnormal lesions from physiological uptake. Eur J Nucl Med Mol Imaging 2020;47:2293-300.
15. de Marco Borges PH, Lizar JC, Faustino ACC, Arruda GV, Pavoni JF. Kurtosis is An MRI Radiomics Feature Predictor of Poor Prognosis in Patients with GBM. Braz J Phys 2021;51:1035-42.
16. Walls GM, Osman SOS, Brown KH, Butterworth KT, Hanna GG, Hounsell AR, McGarry CK, Leijenaar RTH, Lambin P, Cole AJ, Jain S. Radiomics for Predicting Lung Cancer Outcomes Following Radiotherapy: A Systematic Review. Clin Oncol (R Coll Radiol) 2022;34:e107-22.
17. Kirienko M, Sollini M, Corbetta M, Voulaz E, Gozzi N, Interlenghi M, Gallivanone F, Castiglioni I, Asselta R, Duga S, Soldà G, Chiti A. Radiomics and gene expression profile to characterise the disease and predict outcome in patients with lung cancer. Eur J Nucl Med Mol Imaging 2021;48:3643-55.

Cite this article as: Li J, Qiu J, Cheng Z, Lu W. Imaging biomarkers between primary and metastatic tumors revealed by total-body positron emission tomography/computed tomography-based radiomics: a case series. Quant Imaging Med Surg 2024;14(6):4255-4262. doi: 10.21037/qims-24-21